

Successes and Challenges Associated with Solution Processing of Kesterite $\text{Cu}_2\text{ZnSnS}_4$ Solar Cells on Titanium Substrates

Zhengfei Wei^{*a}, Thomas O. Dunlop^a, Peter J. Heard^b, Cecile Charbonneau^a, David A. Worsley^a and Trystan M. Watson^{*a}

^a*SPECIFIC, College of Engineering, Swansea University, Bay Campus, Swansea, SA1 8EN, Wales, U.K.*

^b*Interface Analysis Centre, School of Physics, University of Bristol, Tyndall Avenue, Bristol, BS8 1TL, U.K.*

^{*}) Corresponding Authors: Zhengfei.Wei@swansea.ac.uk and T.M.Watson@swansea.ac.uk

KEYWORDS: CZTS, titanium, solar cell, stress, SIMS

ABSTRACT: Roll-to-roll (R2R) processing of solution-based $\text{Cu}_2\text{ZnSn}(\text{S},\text{Se})_4$ (CZT(S,Se)) solar cells on flexible metal foil is an attractive way to achieve cost-effective manufacturing of photovoltaics. In this work we report the first successful fabrication of solution-processed CZTS devices on a variety of titanium substrates with up to 2.88% power conversion efficiency

(PCE) collected on flexible 75 μm Ti foil. A comparative study of device performance and properties is presented aiming to address key processing challenges. First, we show that a rapid transfer of heat through the titanium substrates is responsible for the accelerated crystallisation of kesterite films characterised with small grain size, a high density of grain boundaries and numerous pore sites near the Mo/CZTS interface which affect charge transport and enhance recombination in devices. Following this, we demonstrate the occurrence of metal ion diffusion induced by the high temperature treatment required for the sulfurization of the CZTS stack: Ti^{4+} ions are observed to migrate upwards to the Mo/CZTS interface whilst Cu^{1+} and Zn^{2+} ions diffuse through the Mo layer into the Ti substrate. Finally, residual stress data confirm the good adhesion of stacked materials throughout the sequential solution process. These findings are evidenced by combining electron imaging observations, elemental depth profiles generated by secondary ion mass spectrometry, and x-ray residual stress analysis of the Ti substrate.

INTRODUCTION

Recent advances in thin film compound semiconductor photovoltaics have demonstrated much of the high potential of these technologies for generating sustainable and cost-efficient energy. Both $\text{Cu}(\text{In},\text{Ga})\text{Se}_2$ (CIGS) and CdTe have achieved power conversion

1
2
3 efficiencies (PCEs) above 20% and they are well developed
4 industrially.¹ Emerging light absorbing materials such as
5 $\text{Cu}_2\text{ZnSn}(\text{S}, \text{Se})_4$ (CZT(S, Se)) only contain earth abundant elements,
6 providing more sustainable alternative to 2nd generation PV
7 technologies. A number of research teams have now successfully
8 fabricated over 10% efficiency CZT(S, Se) solar cell devices at the
9 laboratory scale²⁻⁴, encouraging further development aiming towards
10 higher economic impact.⁵⁻⁶ To address manufacturing costs, light-
11 weight flexible materials such as metal or polymer foils can be
12 used as substrates in roll-to-roll manufacturing. The high power-
13 to-mass ratio of flexible solar cells favours their use in sectors
14 such as building integrated photovoltaics (BIPV), aerospace and
15 automotive power generation, and powering Internet of Things
16 (IoT). Recent advances have been made in the vacuum fabrication of
17 CZT(S, Se) solar cells produced on flexible substrates. For
18 instance, CZT(S, Se) light absorbers were successfully grown
19 directly on stainless steel foil to make photovoltaic devices
20 reaching just over 6% efficiency.⁷⁻⁸ Other metallic substrates such
21 as molybdenum foil⁹⁻¹⁰ and flexible glass¹¹ have been tested with
22 PCEs reaching up to 6.78% and 3.09%, respectively. In comparison,
23 the performance of devices fabricated with solution processed
24 absorbers remains much lower than their vacuum counterpart with
25 cell efficiencies of 1.94% reported on aluminium foil-based
26
27
28
29
30
31
32
33
34
35
36
37
38
39
40
41
42
43
44
45
46
47
48
49
50
51
52
53
54
55
56
57
58
59
60

1
2
3 devices¹², 4.4%¹³ and 2.42%¹⁴ on molybdenum foil, and 0.49% on
4
5 polyimide¹⁵.
6

7
8 Whilst most metal foils appear suitable for roll-to-roll
9
10 manufacturing of PV devices owing to their flexibility and high
11
12 electrical conductivity, other parameters need to be considered
13
14 when optimising the manufacturing CZTS devices. For instance, it
15
16 is desirable that the substrate is characterised with good chemical
17
18 stability and has durable mechanical properties. In addition, the
19
20 behaviour of the metal foil at high temperature (required for the
21
22 preparation of the CZTS film) is also of great importance. In this
23
24 work, we report the first successful preparation of solution-
25
26 processed CZTS solar cells on titanium flexible (thickness: 50 μm
27
28 and 75 μm) and rigid (thickness: 500 μm and 1000 μm) substrates
29
30 (shown in **Figure 1**) and compare their performance to devices built
31
32 on 1 mm soda-lime glass. A two-step stack-building process was
33
34 applied where the active layer was spin-coated from a liquid
35
36 precursor and sulphurisation carried out according to a procedure
37
38 described in previous work.¹⁶⁻¹⁷ Cross sectional electron microscopy
39
40 observations, secondary ion mass spectrometer analysis (SIMS), and
41
42 residual stress analysis of the Ti substrates were applied to
43
44 understand the performance trends in CZTS devices.
45
46
47
48
49
50
51
52
53
54
55
56
57
58
59
60

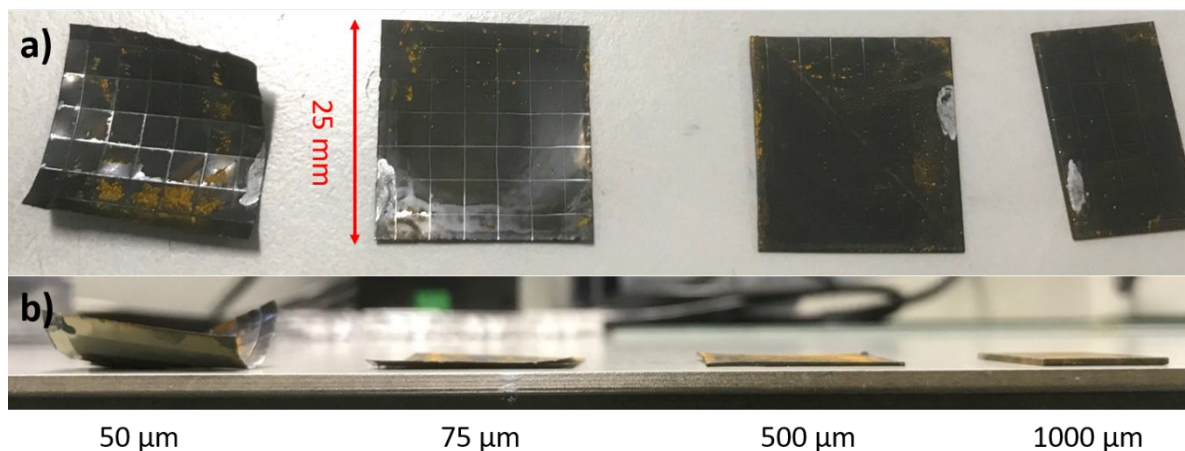


Figure 1. Flexible and rigid CZTS solar cells fabricated on 50-1000 μm Ti substrates: a) top view; b) side view.

EXPERIMENTAL SECTION

1) Substrates and cleaning procedure

Four types of Ti substrates were investigated which thickness (50 μm, 75 μm, 500 μm and 1000 μm), Ti content 99.6-99.9% w.t., and processing have been summarised in **Table S1**, together with those of the control soda-lime glass substrate. Cleaning was operated in an ultrasonic bath sequentially using soap water, deionised water, acetone, and isopropanol. Oxygen plasma treatment followed to remove any residual surface contaminants.

2) Preparation of Mo, CZTS layers, and top contacts

A 400 nm-thick molybdenum (Mo) film was deposited at room temperature by direct current (DC) magnetron sputtering using Kurt Lesker PVD 75 system. The C-Z-T-S precursor solutions were prepared by dissolving $\text{CuCl}_2 \cdot 2\text{H}_2\text{O}$ (98% Alfa Aesar), SnCl_2 (98% Sigma-Aldrich), ZnCl_2 (99.95% Alfa Aesar) and thiourea $\text{SC}(\text{NH}_2)_2$ (99% Sigma-Aldrich) in 5mL DMSO (99.9% Sigma-Aldrich). The $\text{CuCl}_2 \cdot 2\text{H}_2\text{O}$

1
2
3 concentration was 0.55 M and the targeted molar ratio of
4
5 $\text{SnCl}_2:\text{ZnCl}_2:\text{CuCl}_2\cdot 2\text{H}_2\text{O}:\text{thiourea}$ was 1.31:0.69:1:1.84. All the
6
7 precursor solution was doped with 0.14M NaCl. After the back
8
9 contact deposition, the CZTS layers were grown on Mo/Ti substrates
10
11 by spin-coating of the C-Z-T-S solution precursors. Samples were
12
13 subsequently sulphurised in a rapid thermal processing furnace
14
15 (RTP, MTI Corporation) at 560 °C for 20 mins. The thickness of the
16
17 CZTS absorbers was 1.0–1.5 μm . After coating CZTS layers, a ~70 nm
18
19 thick CdS layer was deposited by chemical bath deposition. ZnO
20
21 (~75nm) and Al:ZnO (~500 nm) were radio frequency (RF) sputtered
22
23 with respective power density of 1.87 Wcm^{-2} and 2.46 Wcm^{-2} served
24
25 as a transparent top contact using a Moorfield Nanolab 60
26
27 sputtering system. The transmittance and reflectance of AZO film
28
29 were shown in **Figure S1**. The single cells (0.4 cm x 0.4 cm = 0.16
30
31 cm^2) were defined by manual mechanical scribing.

37 **3) Characterisation of materials and devices**

38
39 Residual stress measurements were carried out with a Bruker D8
40
41 Discover X-ray diffraction system with a 0.07° step size, at a
42
43 time of 7 s per step. The undertaken scans covered the full 0–0.9
44
45 $\sin^2(\psi)$ in both positive and negative ψ tilts to confirm the
46
47 absence of shear stress. Peak evaluation was undertaken using the
48
49 Pearson VII fitting and stresses were calculated using a biaxial
50
51 stress model, assuming $\sigma_{33}=0$.
52
53
54
55
56
57
58
59
60

1
2
3 CZTS/Mo/Ti samples were cross-sectioned using an FEI Helios
4 NanoLab 600 combined focused ion beam/scanning electron
5 microscope. Initially, protective platinum deposits of 20 μm x 2.5
6 μm x 1 μm thickness were made within the instrument using gas-
7 assisted deposition in the presence of a platinum-bearing
8 organometallic gas, in conjunction with a gallium focused ion beam.
9 Vertical trenches (20 μm length x 10 μm width x 10 μm depth) were
10 cut into the materials stack using a gallium focused ion beam of
11 30 keV energy and 20 nA beam. The vertical face of the section was
12 then cleaned with the gallium ion beam at a reduced current of
13 6.5nA to produce high-quality surfaces enabling electron
14 microscopy observations.
15
16
17
18
19
20
21
22
23
24
25
26
27
28
29

30 High magnification (x 25,000) images of the vertical sections
31 were acquired using a JEOL-JSM-7800F field emission scanning
32 electron microscope in secondary electron mode (10 keV beam energy
33 and 0.34 nA beam current, 10 mm WD).
34
35
36
37
38

39 Secondary ion mass spectrometry (SIMS) depth profiles were
40 obtained using an instrument built by the Interface Analysis
41 Centre, at the University of Bristol. This system is featured with
42 an electronically variable aperture type gallium ion gun (FEI SD
43 gallium LMIS EVA focusing column) fitted to a double focusing
44 magnetic sector mass analyser (Vacuum Generators model 7035). The
45 experimental details can be found in our previous report¹⁷. Signals
46 for sodium, titanium, copper, zinc, molybdenum and tin were
47
48
49
50
51
52
53
54
55
56
57
58
59
60

1
2
3 collected with dwell times of 1s per element, cycling through the
4 elements for a total period of 30 minutes.
5

6
7 Current-density-voltage (J - V) curves were measured under
8 simulated AM1.5G spectrum and 100 mW/cm² (1 sun) illumination. The
9 external quantum efficiency (EQE) measurements were performed in
10 AC mode with a chopping frequency of 67 Hz using a QEX10 system
11 (PV Measurements) calibrated with a NIST-certified Si photodiode.
12
13
14
15
16
17
18

19 **RESULTS AND DISCUSSION**

20 **1) Device performance**

21
22 Substrate characteristics including thermal expansion
23 properties, surface roughness, substrate composition and
24 processing condition are critical elements to enable manufacturing
25 of CZTS solar cells on flexible metal substrates.¹⁸⁻²⁰ Here, we
26 selected Ti as our substrate material rather than commonly used
27 stainless steel foil (SS) due to the smaller mismatch of
28 coefficient of thermal expansion (CTE) of Mo/Ti than Mo/SS^{18, 21}
29 and their chemically stability as thin Ti coatings (50-60 nm-
30 thick) were introduced as a diffusion barrier on SS based device
31 in a previous report^{7, 22-23}. We choose rigid (thickness: 500 μ m and
32 1000 μ m) Ti substrate to give a direct comparison to SLG substrate.
33 For most flexible (thickness: 50 μ m) Ti substrate, there is no
34 apparent deformation through the whole coating processes until the
35 mechanical scribing. Some layer-stack were peeled off due to its
36 softness and sensitive to pressure variation caused by mechanical
37
38
39
40
41
42
43
44
45
46
47
48
49
50
51
52
53
54
55
56
57
58
59
60

1
2
3 scribing. The 75 μm -thick Ti foil shows the best flexibility versus
4
5 mechanical stability of fabricated final solar cell device.
6

7
8 The PCE, V_{OC} , J_{SC} , and FF of CZTS cells built on Ti and SLG
9
10 substrates are compared in **Figure 2** and best-performing cells
11
12 parameters summarised in **Table 1**. Overall, cells prepared on
13
14 titanium substrates recorded encouraging outputs with average PCEs
15
16 of 1.49%, 2.08%, 1.81%, and 1.02% for 50, 75, 500, and 1000 μm Ti-
17
18 based cells. The highest Ti-based device performance of 2.88% was
19
20 collected on 75 μm flexible titanium substrate. However, this was
21
22 lower than control SLG-based devices characterised with average
23
24 PCEs of 4.85 % and a maximum at 5.29%. The gap in performance
25
26 between Ti-based and SLG-based devices was associated with an
27
28 important difference in J_{SC} related to high levels of porosity
29
30 (**Figure 3, 4 and S2**) linking with elements diffusion (**Figure 5**)
31
32 and overall higher series resistances (R_s) of Ti-based devices,
33
34 which may stem from the formation of highly resistive secondary
35
36 phases such MoS_2 ²⁴ and Ti_2S_5 ²⁵ at the back contact as evidenced by
37
38 XRD and SIMS (**Figure S3 A, B and Figure 5**). Raman spectra of CZTS
39
40 films prepared on 50, 75, 500, and 1000 μm Ti substrates and on
41
42 SLG (**Figure S3 C and D**) show almost no difference on the spectra
43
44 of these samples, which means three samples have similar
45
46 crystalline phases at CZTS film surface. An examination of samples
47
48 cross sections (**Figure 3, 4 and Figure S2**) revealed that CZTS films
49
50 prepared over Ti substrates had similar thickness ($\sim 1\text{-}1.5 \mu\text{m}$) but
51
52
53
54
55
56
57
58
59
60

1
2
3 smaller grain size (< 200 nm) compared to films produced on SLG
4 (up to 700-800 nm). Smaller crystals and higher densities of grain
5 boundaries have been shown to hinder charge transport across CZTS
6 films²⁶⁻²⁷ and are here responsible for decreased R_{SH} . The Ti-based
7 films also displayed high levels of porosity compared to SLG-based
8 films. The absence of active material in pore sites greatly
9 affected the density of charges produced and impacted on average
10 device J_{SC} . This was in good agreement with the EQE data which
11 confirmed lower levels of charge generation across the entire
12 wavelength range (Figure 2). Higher levels of charge recombination
13 evidenced by lower R_{sh} data, J_{SC} and fill factor were assigned to
14 the enhanced density of CZTS/void and CZTS/CZTS grain boundaries
15 which are prone to defects and known to act as recombination
16 sites.²⁷⁻²⁸ Finally, the V_{OC} of Ti-based devices, ranging between
17 0.40-0.47 V, was also found to be systematically lower than the
18 V_{OC} of SLG-based devices averaging 0.57 V. EQE data (**Figure 2**)
19 demonstrated very little variations in the bandgap of CZTS films
20 across all samples (1.547-1.575 eV for the Ti-based films compared
21 to 1.562 eV for the SLG-based film). Hence, we suspect the
22 difference in V_{OC} is attributed to the formation of a thicker MoS_2
23 layer⁷ enabled by the effective conduction of heat through Ti
24 substrates. This is evidenced by increased R_s which is caused by
25 high resistivity of the thick MoS_2 layer²⁹ and XRD peaks at 26°
26 and
27
28
29
30
31
32
33
34
35
36
37
38
39
40
41
42
43
44
45
46
47
48
49
50
51
52
53
54
55
56
57
58
59
60

1
2
3 32° in Ti-based devices as compared to SLG-based devices²⁴ (**Table**
4
5 **S2 and Figure S3 A and B**).

6
7 A comparison of photovoltaic performance for Ti-based devices
8 only showed little effect of the substrate thickness. However,
9
10 devices built over 50 μm and 1000 μm Ti substrates were
11
12 characterised with lower average PCEs of 1.49 % and 1.02% compared
13
14 to 2.08 % and 1.81 % for devices built over 75 μm and 500 μm Ti
15
16 substrates. In the case of devices prepared on Ti-1000 μm, lower
17
18 average FF and R_{sh} were assigned to localized delamination between
19
20 the Mo and Ti layers in areas characterised with higher interface
21
22 roughness, as illustrated in **Figure 3e**. The lower performance of
23
24 devices prepared on 50 μm Ti substrates was attributed to the
25
26 mechanical failure of the CZTS stack near mechanically scribed
27
28 cell edges. The local deformation of the substrate, evidenced by
29
30 the formation of ridges apparent at the top edge of the sample in
31
32 **Figure 1a**, is thought to be responsible for the loss of CZTS
33
34 material which translated into lower average J_{sc} . The other
35
36 samples, built on far less flexible Ti substrates, remained
37
38 unaffected by this process.
39
40
41
42
43
44
45
46
47
48
49
50
51
52
53
54
55
56
57
58
59
60

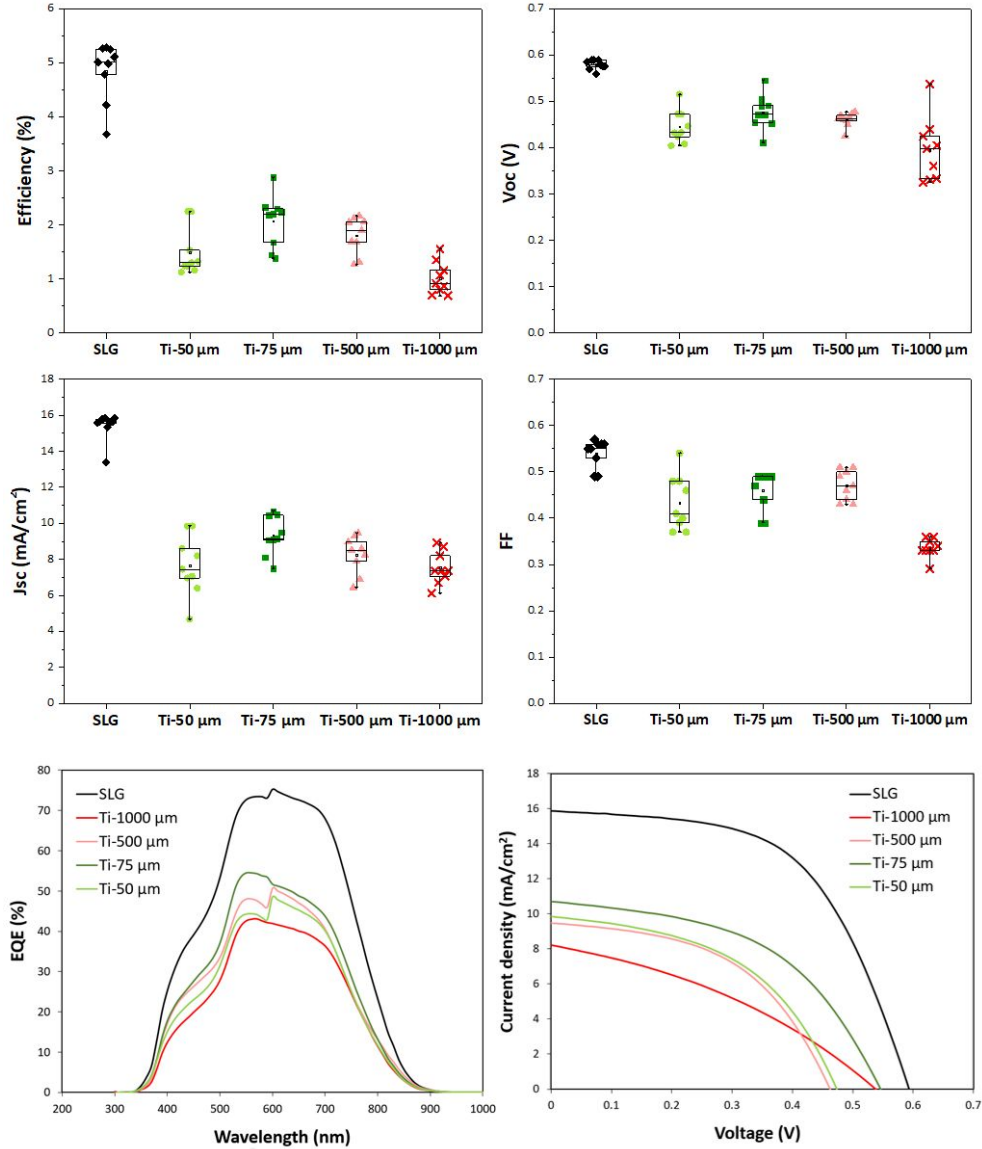


Figure 2. Box plots of J-V characteristics for CZT(S,Se) devices prepared on soda-lime glass (SLG) and 50, 75, 500, and 1000 μm Ti substrates.

Table 1. Summary of device parameters for the average values and the best-performing values of CZTS solar cells fabricated on 50, 75, 500, and 1000 μm Ti substrates and SLG.

Substrate	η		V_{oc}		J_{sc}		FF	
	(%)		(V)		$(\text{mA}\cdot\text{cm}^{-2})$			
Glass (SLG)	4.84 \pm 0.55	5.29	0.58 \pm 0.01	0.59	15.41 \pm 0.78	15.87	0.54 \pm 0.03	0.56
Ti-50 μm	1.49 \pm 0.45	2.25	0.45 \pm 0.04	0.47	7.67 \pm 1.67	9.85	0.43 \pm 0.06	0.48
Ti-75 μm	2.08 \pm 0.48	2.88	0.48 \pm 0.04	0.55	9.34 \pm 1.08	10.69	0.46 \pm 0.04	0.49
Ti-500 μm	1.81 \pm 0.34	2.17	0.46 \pm 0.02	0.46	8.25 \pm 1.03	9.45	0.47 \pm 0.03	0.50
Ti-1000μm	1.02 \pm 0.30	1.56	0.40 \pm 0.07	0.54	7.54 \pm 0.92	8.20	0.34 \pm 0.02	0.35

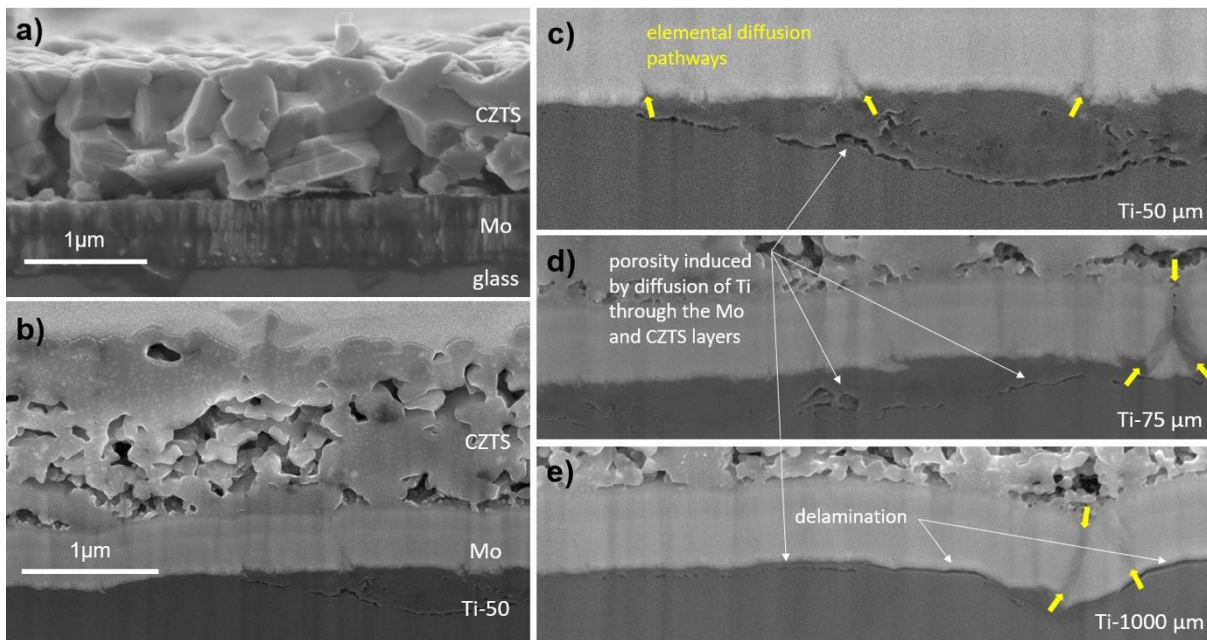


Figure 3. Cross-section SEM images of CZTS samples on (a) Mo/SLG-1000 μm ; (b) Mo/Ti-50 μm . Selected areas of CZTS devices prepared on Ti substrates highlighting Ti diffusion pathways, residual Ti-

1
2
3 porosity and areas of delamination: (c) Mo/Ti-50 μm ; (d) Mo/Ti-75
4
5 μm ; (e) Mo/Ti-1000 μm .
6
7
8
9

10 **2) Manufacturing challenges for Ti-based CZTS devices**

11
12 Controlling the crystallisation of the CZTS layer to achieve
13
14 large grains is critical to obtain efficient charge transport and
15
16 optimum device performance.^{26, 28} Various deposition methods have
17
18 been developed to address these processing challenges.⁷⁻⁹ In the
19
20 case of solution processed films, it was demonstrated that is
21
22 particularly important to tailor the heat treatment applied during
23
24 this fabrication stage.⁹ Here, a CZTS precursor containing metal
25
26 chloride salts was spin coated onto Mo/Ti substrates and
27
28 sulphurised in a rapid thermal processing furnace at 560 °C for 20
29
30 mins. Despite the great care taken in optimizing this process for
31
32 SLG-based devices¹⁶⁻¹⁷ results here show that further work is needed
33
34 to achieve similar CZTS films on Ti substrates. As previously
35
36 mentioned, a comparison of CZTS film cross-sections **Figure 3a** and
37
38 **Figure 3b** showed overall much smaller crystals in Ti-based samples
39
40 compared to SLG-based samples. A systematic assessment of crystal
41
42 size across samples showed that all Ti-based samples were
43
44 characterised with smaller CZTS crystals near the Mo/CZTS
45
46 interface compared to the top part of the film. This has been
47
48 evidenced in **Figure 4** where coloured areas highlight the occurrence
49
50 of < 100 nm size crystals at the bottom of the films (in blue)
51
52 and
53
54
55
56
57
58
59
60

1
2
3 over > 150 nm crystals (in red) at the centre and top parts of the
4
5 films. An increasing crystal size upwards through the CZTS film
6
7 suggests a gradient in the nucleation rate. This was not the case
8
9 of SLG-based CZTS film where the size distribution of crystals was
10
11 much larger and consistent across the thickness of the film.
12
13 Titanium is known to conduct heat a lot more effectively than glass
14
15 with a thermal conduction coefficient of 24 W/m·K, almost 25 times
16
17 higher than soda lime glass ranging between 0.7-1.3 W/m·K. Here,
18
19 we can conclude that the temperature of Ti substrates raised faster
20
21 than that of the SLG substrate, causing an acceleration of
22
23 nucleation events at the bottom of the films. In terms of
24
25 manufacturing, there may be an opportunity to develop low heat
26
27 conduction layers allowing a finer control over CZTS
28
29 crystallization. Alternately, the heat treatment applied to
30
31 sulphurize the CZTS film should be optimized based on the nature
32
33 of the substrate. Whilst the temperature profile of the
34
35 sulphurization process may be adjusted, it may be of interest to
36
37 investigate the application of selective heating techniques such
38
39 as demonstrated for the crystallisation of perovskite light
40
41 absorbers.³⁰
42
43
44
45
46
47
48
49
50
51
52
53
54
55
56
57
58
59
60

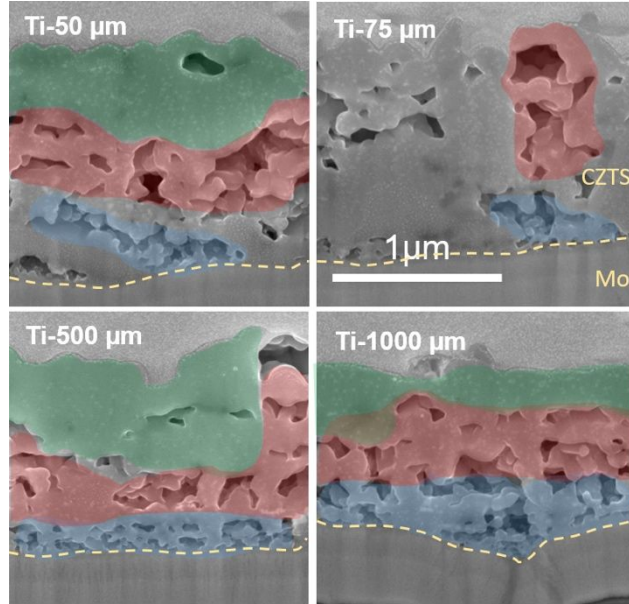


Figure 4. FEG-SEM cross sectional views of CZTS films built over Ti substrates highlighting areas characterised with small CZTS crystals (blue), large CZTS crystals (red), low levels of porosity (green).

Another challenge for the manufacturing of efficient metal-based CZTS devices is the diffusion of elements across layers of materials. The sulfurization of the molybdenum layer, an unwanted side effect of the high temperature sulphurization process, is already well documented.^{17, 29, 31} But there are fewer published accounts addressing the diffusion of other elements, namely metallic ions.^{7-8, 22} Sun *et al.* reported on the use of a Ti barrier layer aiming to prevent the diffusion of substrate Fe ions to the CZTS film.⁷ To confirm the suitability of Ti with this regard, we investigated the motion of Ti ions of Ti-based CZTS stacks by combining cross-section imaging observations and secondary ion

1
2
3 mass spectrometry elemental depth profiling. At high
4
5 magnification, the examination of the Mo/Ti interface (**Figure 5.a-**
6
7 **d)** revealed the presence of pores in the Ti layer near the
8
9 interface. Directly above these in the Mo layer, darker linear
10
11 contrasts indicative of lower atomic weight elements was observed,
12
13 sometimes extending across the entire thickness of the Mo layer.
14
15 These strongly suggested the diffusion of Ti ions upwards areas,
16
17 causing the formation of pores at the top of the Ti layer. These
18
19 features were particularly pronounced in Ti-50 μm and Ti-75 μm
20
21 stacks where heat conduction was more effective than in much
22
23 thicker Ti-500 μm and Ti-1000 μm . This hypothesis was further
24
25 confirmed by SIMS depth profile data. **Figure 6** shows elemental
26
27 signals collected for Cu, Sn, Zn, Ti, Mo, and Na plotted against
28
29 the etching time. All samples exhibited common features: 1) between
30
31 0-250 s etching time, high levels of Cu, Zn, and Sn were recorded
32
33 which were assigned to the CZTS layer; 2) between 250-550 s etching
34
35 time, decreasing levels of Cu, Zn, and Sn but high levels of Na
36
37 and Mo suggested a transition to the Na-doped Mo layer; 3) over
38
39 550s etching time, the Ti signal became predominant as the etching
40
41 gun reached the top of the metallic substrate. Similar elemental
42
43 profiles had been collected for a SLG-Mo-CZTS stack in previous
44
45 work.¹⁷ However, in thin Ti-50 and Ti-75 μm substrates, a peak in
46
47 Ti signal intensity was observed at approximately 300s, suggesting
48
49 the accumulation of Ti atoms near the CZTS/Mo interface. This
50
51
52
53
54
55
56
57
58
59
60

1
2
3 confirms the diffusion of Ti across the Mo layer for these two
4 samples (**Figure 3c** and **Figure 3d**). The same Ti peak was absent
5
6 from depth profiles of samples built over thick Ti-500 and Ti-1000
7
8 μm substrates for which heat transfer was too slow to cause as
9
10 significant diffusion of Ti (**Figure 5c** and **Figure 5d**). Another
11
12 important finding relates to Cu and Zn elemental signals increasing
13
14 after 500s of etching time, indicative the high concentrations of
15
16 these elements at the Mo/Ti interface and in the depth of the Ti
17
18 substrate. Increased Cu and Zn signals over 550s likely stems from
19
20 oxygen enhancement effects (so called SIMS matrix effects) by
21
22 formation of TiO_2 between the Mo layer and Ti substrate.³²⁻³⁴ This
23
24 suggests the occurrence of an inverse diffusion phenomenon where
25
26 the upwards movement of Ti^{4+} ions was compensated by downwards
27
28 migrations of Cu^{1+} and Zn^{2+} ions, possibly through the same pathways
29
30 (**Figure 5b & 5c**). The diffusion of Cu and Zn also correlate higher
31
32 densities of pores observed at the bottom of the CZTS film (**Figure**
33
34 **4** - blue areas) compared to the top of the films generally
35
36 characterised with lower levels of porosity (**Figure 4** - green
37
38 areas).

39
40
41
42
43
44
45
46
47
48
49
50
51
52
53
54
55
56
57
58
59
60

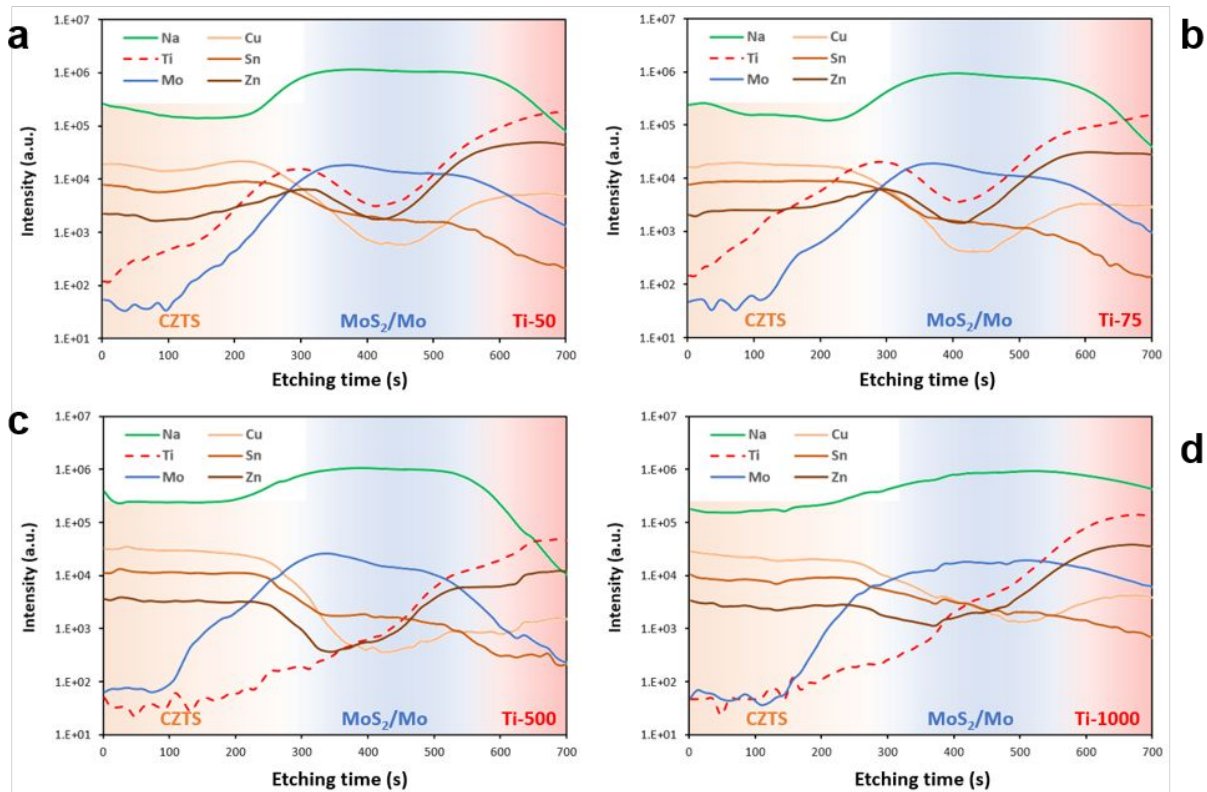


Figure 5. SIMS elemental depth profiles of CZTS samples on Ti substrates: (a) Mo/Ti-50 μm ; (b) Mo/Ti-75 μm ; (c) Mo/Ti-500 μm ; (d) Mo/Ti-1000 μm CZTS, MoS_2/Mo and Ti are shown with orange, blue and red backgrounds, respectively.

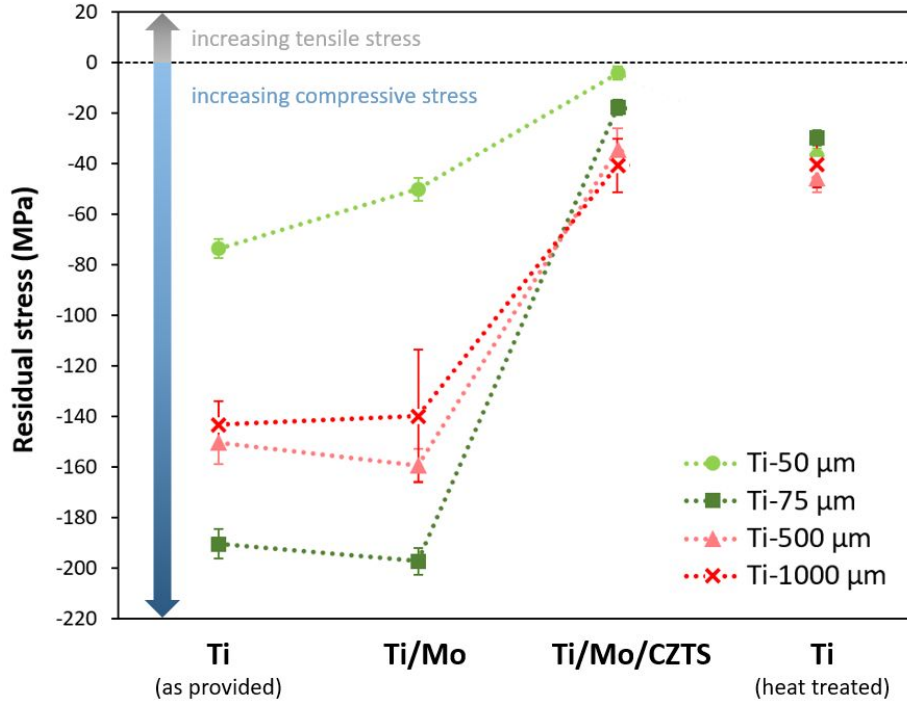


Figure 6. Residual stress analysis of Ti substrates in the σ_{11} direction using a biaxial model, following the application of a Mo layer (Mo/Ti), after the deposition and sulphurisation of the CZTS layer at 560 °C for 20 mins (CZTS/Mo/Ti), and for bare Ti substrates heated at 560 °C for 20min.

The mechanical stability of stacked layers of materials plays an important role in ensuring a successful transfer of photovoltaic technologies from lab scale to large roll-to-roll manufacturing. In previous work¹⁷, we demonstrated that the sequential deposition of thin layers of Si_xN_y over Mo could induce compressive stress inside the Mo layer later on responsible for the delamination of the CZTS layer. In this work, the mechanical stability of our stacked layers was assessed by collecting x-ray residual stress

1
2
3 (σ_{11} and σ_{22} directions) data generated at the surface of the Ti
4 layer, at each stage of the stack building process. Results
5 presented in **Figure 6** indicate that all Ti substrates initially
6 held compressive stresses of varying magnitude induced by the
7 rolling of Ti bulk material into sheets and foils; this is despite
8 the annealing treatment provided at the end of the manufacturing
9 process which usually aims to release some of these stresses by
10 promoting the re-organisation of the metallic crystalline matrix
11 at high temperature. The data collected for Ti/Mo samples show
12 that the deposition of a 400 nm Mo layer, operated at ambient
13 temperature, had little effect over surface stress for most samples
14 except for the Ti-50 μm samples which compressive stress decreased
15 by 26% from -76.4 ± 2.6 MPa to -58.1 ± 4.2 MPa. However, the deposition
16 and sulphurisation of the CZTS layer operated at 560 °C for 20
17 mins drastically reduced surface compressive stress in all Ti
18 substrates. In particular, flexible Ti/Mo/CZTS samples with built
19 on Ti-50 μm and Ti-75 μm displayed > 90 % loss whilst rigid samples
20 built on Ti-500 μm and Ti-1000 μm displayed close to 75 % loss in
21 surface compressive stress compared to their initial (Ti, as
22 provided) state. The difference in stress release experienced by
23 flexible compared to rigid Ti substrates may be assigned to faster
24 temperature rise of the surface in the thinner substrates. The
25 relaxation of Ti substrates throughout the stack building steps
26 correlates the good mechanical adhesion observed between the Ti
27
28
29
30
31
32
33
34
35
36
37
38
39
40
41
42
43
44
45
46
47
48
49
50
51
52
53
54
55
56
57
58
59
60

1
2
3 and Mo layers in all samples. Hence, localised short ranged
4 delamination features observed at the Ti/Mo interface of the Ti-
5
6 1000 μm sample (**Figure 3e**) are mostly assigned to locally high
7
8 roughness. Further testing was carried out on Ti substrates taken
9
10 at 560 °C for 20 mins in the absence of other materials to confirm
11
12 the impact of heat over the relaxation of Ti. As expected, we found
13
14 that compressive stress was drastically reduced in heat-treated
15
16 samples. However, it was not reduced as much as in Ti substrates
17
18 of Ti/Mo/CZTS samples. This suggests that in the stack of
19
20 materials, the re-organisation of Ti atoms at the surface of the
21
22 Ti substrate was more efficient, supported by the bi-directional
23
24 diffusion of metallic ions, namely Ti^{4+} , Cu^{1+} , and Zn^{2+} ions.
25
26
27
28
29

30 CONCLUSIONS

31
32 With this work we demonstrated the successful solution processing
33
34 of CZTS solar cells on flexible Ti substrate with up to 2.88% power
35
36 conversion efficiency achieved on 75 μm thick foil. Whilst this was
37
38 achieved on a metal substrate readily usable for roll-to-roll
39
40 manufacturing, specific issues related materials processing were
41
42 highlighted. The unexpectedly efficient conduction of heat through
43
44 the Ti substrate (compared to a sodium lime glass substrate, even
45
46 at comparable thickness) led to the fast nucleation of CZTS
47
48 crystals at the bottom of the layer, favouring the formation of
49
50 small crystals and pores which are detrimental to device
51
52 efficiency. The top of the films crystalized much slower and
53
54
55
56
57
58
59
60

1
2
3 displayed larger crystals together with lower levels of porosity.
4
5 Another undesirable phenomenon related to the diffusion of
6
7 metallic ions: we observed the diffusion of Ti^{4+} ions from the
8
9 substrate to the bottom part of the CZTS film whilst Cu^{1+} and Zn^{2+}
10
11 leached out of the film and diffused downwards to the metallic
12
13 substrate, contributing to further porosity. However, this may be
14
15 prevented by introducing barrier layers, a method already
16
17 successfully reported to minimize the conversion of Mo to MoS_2 .¹⁷
18
19 In terms of device characteristics, increased recombination and
20
21 resistance losses were found in the bulk of the CZTS film prepared
22
23 on Ti substrates compared to SLG-based devices. These were
24
25 associated with thermally induced porosity and high density of
26
27 grain boundaries, pronounced MoS_2 formation and metallic ions
28
29 diffusion. These results suggest that further optimization of the
30
31 sulfurisation process is necessary and may result in the
32
33 fabrication of devices with outputs comparable to SLG-based
34
35 devices.
36
37
38
39
40
41
42
43

44 **ASSOCIATED CONTENT**

45
46 **Supporting Information** Available: Characteristics of substrates,
47
48 Transmittance and reflectance of AZO film, SEM images and
49
50 photovoltaic performance parameters of the CZTS devices fabricated
51
52 with different Ti substrate thicknesses are presented. This
53
54
55
56
57
58
59
60

1
2
3 material is available free of charge via the Internet at
4
5 <http://pubs.acs.org>.
6

7
8 **ORCID:**

9
10 Zhengfei Wei: 0000-0002-4358-9287

11
12 Thomas O. Dunlop: 0000-0002-5851-8713

13
14 Peter J. Heard: 0000-0002-8926-4680

15
16 Cecile Charbonneau: 0000-0001-9887-2007

17
18 David A. Worsley: 0000-0002-9956-6228

19
20 Trystan M. Watson: 0000-0002-8015-1436
21
22
23
24
25
26
27

28 **ACKNOWLEDGMENTS**

29
30 The IMPACT operation has been part-funded by the European
31
32 Regional Development Fund through the Welsh Government and Swansea
33
34 University. The authors would like to thank the financial support
35
36 provided by Engineering and Physical Sciences Research Council
37
38 (EPSRC) through the SPECIFIC Innovation and Knowledge Centre Phase
39
40 2 (EP/ N020863/1) and Photovoltaic Technology based on Earth
41
42 Abundant Materials - PVTEAM project (EP/L017792/1). We would like
43
44 to acknowledge the assistance provided by Swansea University
45
46 College of Engineering AIM Facility, which was funded in part by
47
48 the EPSRC (EP/M028267/1), the European Regional Development Fund
49
50 through the Welsh Government (80708) and the Ser Solar project via
51
52 Welsh Government.
53
54
55
56
57
58
59
60

REFERENCES

- 1
2
3
4
5
6
7
8
9
10
11
12
13
14
15
16
17
18
19
20
21
22
23
24
25
26
27
28
29
30
31
32
33
34
35
36
37
38
39
40
41
42
43
44
45
46
47
48
49
50
51
52
53
54
55
56
57
58
59
60
- (1) Green, M. A.; Hishikawa, Y.; Dunlop, E. D.; Levi, D. H.; Hohl-Ebinger, J.; Ho-Baillie, A. W. Y. Solar cell efficiency tables (version 52). *Progress in Photovoltaics: Research and Applications* **2018**, *26* (7), 427-436, DOI: doi:10.1002/pip.3040.
- (2) Wang, W.; Winkler, M. T.; Gunawan, O.; Gokmen, T.; Todorov, T. K.; Zhu, Y.; Mitzi, D. B. Device Characteristics of CZTSSe Thin-Film Solar Cells with 12.6% Efficiency. *Advanced Energy Materials* **2014**, *4* (7), n/a-n/a, DOI: 10.1002/aenm.201301465.
- (3) Yan, C.; Huang, J.; Sun, K.; Johnston, S.; Zhang, Y.; Sun, H.; Pu, A.; He, M.; Liu, F.; Eder, K.; Yang, L.; Cairney, J. M.; Ekins-Daukes, N. J.; Hameiri, Z.; Stride, J. A.; Chen, S.; Green, M. A.; Hao, X. Cu₂ZnSnS₄ solar cells with over 10% power conversion efficiency enabled by heterojunction heat treatment. *Nature Energy* **2018**, *3* (9), 764-772, DOI: 10.1038/s41560-018-0206-0.
- (4) Xin, H.; Vorpahl, S. M.; Collord, A. D.; Braly, I. L.; Uhl, A. R.; Krueger, B. W.; Ginger, D. S.; Hillhouse, H. W. Lithium-doping inverts the nanoscale electric field at the grain boundaries in Cu₂ZnSn(S,Se)₄ and increases photovoltaic efficiency. *Physical Chemistry Chemical Physics* **2015**, *17* (37), 23859-23866, DOI: 10.1039/C5CP04707B.
- (5) Jäger-Waldau, A. Market Challenges for CZTS-Based Thin-Film Solar Cells. In *Copper Zinc Tin Sulfide-Based Thin-Film Solar Cells*; Ito, K., Ed.; John Wiley & Sons Ltd: 2015; pp 43-51.
- (6) Eslamian, M. Inorganic and Organic Solution-Processed Thin Film Devices. *Nano-Micro Letters* **2016**, *9* (1), 3, DOI: 10.1007/s40820-016-0106-4.
- (7) Sun, K.; Liu, F.; Huang, J.; Yan, C.; Song, N.; Sun, H.; Xue, C.; Zhang, Y.; Pu, A.; Shen, Y.; Stride, J. A.; Green, M.; Hao, X. Flexible kesterite Cu₂ZnSnS₄ solar cells with sodium-doped molybdenum back contacts on stainless steel substrates. *Solar Energy Materials and Solar Cells* **2018**, *182*, 14-20, DOI: <https://doi.org/10.1016/j.solmat.2018.02.036>.
- (8) López-Marino, S.; Sánchez, Y.; Espíndola-Rodríguez, M.; Alcobé, X.; Xie, H.; Neuschitzer, M.; Becerril, I.; Giraldo, S.; Dimitrievska, M.; Placidi, M.; Fourdrinier, L.; Izquierdo-Roca, V.; Pérez-Rodríguez, A.; Saucedo, E. Alkali doping strategies for flexible and light-weight Cu₂ZnSnSe₄ solar cells. *Journal of Materials Chemistry A* **2016**, *4* (5), 1895-1907, DOI: 10.1039/C5TA09640E.
- (9) Yan, Q.; Cheng, S.; Li, H.; Yu, X.; Fu, J.; Tian, Q.; Jia, H.; Wu, S. High flexible Cu₂ZnSn(S,Se)₄ solar cells by green solution-process. *Solar Energy* **2019**, *177*, 508-516, DOI: <https://doi.org/10.1016/j.solener.2018.11.030>.

- 1
2
3 (10) Jo, E.; Gang, M. G.; Shim, H.; Suryawanshi, M. P.;
4 Ghorpade, U. V.; Kim, J. H. 8% Efficiency Cu₂ZnSn(S,Se)₄
5 (CZTSSe) Thin Film Solar Cells on Flexible and Lightweight
6 Molybdenum Foil Substrates. *ACS Applied Materials & Interfaces*
7 **2019**, DOI: 10.1021/acsami.9b03195.
8
9 (11) Peng, C.-Y.; Dhakal, T. P.; Garner, S.; Cimo, P.; Lu, S.;
10 Westgate, C. R. Fabrication of Cu₂ZnSnS₄ solar cell on a
11 flexible glass substrate. *Thin Solid Films* **2014**, 562, 574-577,
12 DOI: <https://doi.org/10.1016/j.tsf.2014.03.054>.
13
14 (12) Tian, Q.; Xu, X.; Han, L.; Tang, M.; Zou, R.; Chen, Z.; Yu,
15 M.; Yang, J.; Hu, J. Hydrophilic Cu₂ZnSnS₄ nanocrystals for
16 printing flexible, low-cost and environmentally friendly solar
17 cells. *CrystEngComm* **2012**, 14 (11), 3847-3850, DOI:
18 10.1039/C2CE06552E.
19
20 (13) Xu, X.; Qu, Y.; Campbell, S.; Le Garrec, M.; Ford, B.;
21 Barrioz, V.; Zoppi, G.; Beattie, N. S. Solution processing route
22 to Na incorporation in CZTSSe nanoparticle ink solar cells on
23 foil substrate. *Journal of Materials Science: Materials in*
24 *Electronics* **2019**, 30 (8), 7883-7889, DOI: 10.1007/s10854-019-
25 01108-3.
26
27 (14) Sun, K.; Su, Z.; Yan, C.; Liu, F.; Cui, H.; Jiang, L.;
28 Shen, Y.; Hao, X.; Liu, Y. Flexible Cu₂ZnSnS₄ solar cells based
29 on successive ionic layer adsorption and reaction method. *RSC*
30 *Advances* **2014**, 4 (34), 17703-17708, DOI: 10.1039/C3RA47823H.
31
32 (15) Zhou, Z.; Wang, Y.; Xu, D.; Zhang, Y. Fabrication of
33 Cu₂ZnSnS₄ screen printed layers for solar cells. *Solar Energy*
34 *Materials and Solar Cells* **2010**, 94 (12), 2042-2045, DOI:
35 <https://doi.org/10.1016/j.solmat.2010.06.010>.
36
37 (16) Wei, Z.; Zhu, M.; McGettrick, J. D.; Kissling, G. P.;
38 Peter, L. M.; Watson, T. M. The effect of additional sulfur on
39 solution-processed pure sulfide Cu₂ZnSnS₄ solar cell absorber
40 layers. *MRS Advances* **2016**, FirstView, 1-6, DOI:
41 doi:10.1557/adv.2016.425.
42
43 (17) Wei, Z.; Fung, C. M.; Pockett, A.; Dunlop, T. O.;
44 McGettrick, J. D.; Heard, P. J.; Guy, O. J.; Carnie, M. J.;
45 Sullivan, J. H.; Watson, T. M. Engineering of a Mo/SixNy
46 Diffusion Barrier to Reduce the Formation of MoS₂ in Cu₂ZnSnS₄
47 Thin Film Solar Cells. *ACS Applied Energy Materials* **2018**, 1 (6),
48 2749-2757, DOI: 10.1021/acsaem.8b00401.
49
50 (18) Kessler, F.; Rudmann, D. Technological aspects of flexible
51 CIGS solar cells and modules. *Solar Energy* **2004**, 77 (6), 685-
52 695, DOI: <https://doi.org/10.1016/j.solener.2004.04.010>.
53
54 (19) Zhang, Y.; Ye, Q.; Liu, J.; Chen, H.; He, X.; Liao, C.;
55 Han, J.; Wang, H.; Mei, J.; Lau, W. Earth-abundant and low-cost
56 CZTS solar cell on flexible molybdenum foil. *RSC Advances* **2014**,
57 4 (45), 23666-23669, DOI: 10.1039/C4RA02064B.
58
59
60

- 1
2
3 (20) Brémaud, D.; Rudmann, D.; Kaelin, M.; Ernits, K.; Bilger,
4 G.; Döbeli, M.; Zogg, H.; Tiwari, A. N. Flexible Cu(In,Ga)Se₂ on
5 Al foils and the effects of Al during chemical bath deposition.
6 *Thin Solid Films* **2007**, 515 (15), 5857-5861, DOI:
7 <https://doi.org/10.1016/j.tsf.2006.12.152>.
8
9 (21) Yazici, S.; Olgar, M. A.; Akca, F. G.; Cantas, A.; Kurt,
10 M.; Aygun, G.; Tarhan, E.; Yanmaz, E.; Ozyuzer, L. Growth of
11 Cu₂ZnSnS₄ absorber layer on flexible metallic substrates for
12 thin film solar cell applications. *Thin Solid Films* **2015**, 589,
13 563-573, DOI: <https://doi.org/10.1016/j.tsf.2015.06.028>.
14
15 (22) Blösch, P.; Pianezzi, F.; Chirilă, A.; Rossbach, P.;
16 Nishiwaki, S.; Buecheler, S.; Tiwari, A. N. Diffusion barrier
17 properties of molybdenum back contacts for Cu(In,Ga)Se₂ solar
18 cells on stainless steel foils. *Journal of Applied Physics* **2013**,
19 113 (5), 054506, DOI: 10.1063/1.4789616.
20
21 (23) Buldu, D. G.; Cantas, A.; Turkoglu, F.; Akca, F. G.; Meric,
22 E.; Ozdemir, M.; Tarhan, E.; Ozyuzer, L.; Aygun, G. Influence of
23 sulfurization temperature on Cu₂ZnSnS₄ absorber layer on
24 flexible titanium substrates for thin film solar cells. *Physica*
25 *Scripta* **2018**, 93 (2), 024002, DOI: 10.1088/1402-4896/aa95eb.
26
27 (24) Olgar, M. A.; Tomakin, M.; Kucukomeroglu, T.; Bacaksız, E.
28 Growth of Cu₂ZnSnS₄ (CZTS) thin films using short sulfurization
29 periods. *Materials Research Express* **2019**, 6 (5), 056401, DOI:
30 10.1088/2053-1591/aaff78.
31
32 (25) Owens, J. P.; Conrad, B. R.; Franzen, N. F. The crystal
33 structure of Ti₂S. *Acta Crystallographica* **1967**, 23 (1), 77-82,
34 DOI: 10.1107/s0365110x67002154.
35
36 (26) Wei, Z. Process development and optimisation for efficient
37 and cost-effective Cu(In,Ga)Se₂ thin film solar cells. PhD
38 thesis, Heriot-Watt University Edinburgh, 2014.
39
40 (27) Sardashti, K.; Haight, R.; Gokmen, T.; Wang, W.; Chang, L.-
41 Y.; Mitzi, D. B.; Kummel, A. C. Impact of Nanoscale Elemental
42 Distribution in High-Performance Kesterite Solar Cells. *Advanced*
43 *Energy Materials* **2015**, 5 (10), 1402180, DOI:
44 10.1002/aenm.201402180.
45
46 (28) Bourdais, S.; Choné, C.; Delatouche, B.; Jacob, A.;
47 Larramona, G.; Moisan, C.; Lafond, A.; Donatini, F.; Rey, G.;
48 Siebentritt, S.; Walsh, A.; Dennler, G. Is the Cu/Zn Disorder
49 the Main Culprit for the Voltage Deficit in Kesterite Solar
50 Cells? *Advanced Energy Materials* **2016**, n/a-n/a, DOI:
51 10.1002/aenm.201502276.
52
53 (29) Scragg, J. J.; Wätjen, J. T.; Edoff, M.; Ericson, T.;
54 Kubart, T.; Platzer-Björkman, C. A Detrimental Reaction at the
55 Molybdenum Back Contact in Cu₂ZnSn(S,Se)₄ Thin-Film Solar Cells.
56 *Journal of the American Chemical Society* **2012**, 134 (47), 19330-
57 19333, DOI: 10.1021/ja308862n.
58
59
60

(30) Troughton, J.; Carnie, M. J.; Davies, M. L.; Charbonneau, C.; Jewell, E. H.; Worsley, D. A.; Watson, T. M. Photonic flash-annealing of lead halide perovskite solar cells in 1 ms. *Journal of Materials Chemistry A* **2016**, *4* (9), 3471-3476, DOI: 10.1039/C5TA09431C.

(31) Scragg, J. J.; Kubart, T.; Wätjen, J. T.; Ericson, T.; Linnarsson, M. K.; Platzer-Björkman, C. Effects of Back Contact Instability on Cu₂ZnSnS₄ Devices and Processes. *Chemistry of Materials* **2013**, *25* (15), 3162-3171, DOI: 10.1021/cm4015223.

(32) Yu, M. L. Chemical enhancement effects in SIMS analysis. *Nuclear Instruments and Methods in Physics Research Section B: Beam Interactions with Materials and Atoms* **1986**, *15* (1), 151-158, DOI: [https://doi.org/10.1016/0168-583X\(86\)90273-9](https://doi.org/10.1016/0168-583X(86)90273-9).

(33) Vickerman, J. C. Secondary ion mass spectrometry-basic concepts, instrumental aspects, applications and trends. A. BENNINGHOVEN, F. G. RUDENAUER and H. W. WERNER, Wiley, New York, 1987, 1277 pages. *Surface and Interface Analysis* **1987**, *10* (8), 435-435, DOI: 10.1002/sia.740100811.

(34) Oueslati, S.; Brammertz, G.; Buffière, M.; ElAnzeery, H.; Mangin, D.; ElDaif, O.; Touayar, O.; Köble, C.; Meuris, M.; Poortmans, J. Study of alternative back contacts for thin film Cu₂ZnSnSe₄-based solar cells. *Journal of Physics D: Applied Physics* **2014**, *48* (3), 035103, DOI: 10.1088/0022-3727/48/3/035103.

Graphical abstract

